Nanoscale Research Letters

NANO IDEA Open Access

Adsorption of SF_6 Decomposed Products on ZnO-Modified C_3N: A Theoretical Study

Peng Wu[1], Xiaoxing Zhang[1,2,3*], Dachang Chen[1] and Ju Tang[1]

Abstract

SF_6, as an outstanding insulation medium, is widely used in the high-voltage insulation devices, guaranteeing the safe operation of the power system. Nevertheless, the inevitable partial discharge in a long-running device causes the decomposition of SF_6 and deteriorates its insulation performance. In this work, DFT calculations were performed to study the adsorbing and sensing properties of ZnO-modified C_3N (ZnO-C_3N) nanosheet towards SF_6 decomposed products, in order to propose a novel nano-candidate for evaluating the operation status of SF_6 insulation devises. We first investigated the structure of ZnO-C_3N monolayer and then simulated its adsorption behaviour upon four typical SF_6 decomposed species, namely H_2S, SO_2, SOF_2, and SO_2F_2. It is found that the ZnO-C_3N monolayer can exhibit desirable reactivity and sensitivity on SO_2, SOF_2, and SO_2F_2, leading to the intense deformation of gas molecules and large adsorption energies. These consequences allow the potential application of gas adsorbent based on ZnO-C_3N monolayer for removing impurity gases from SF_6 insulation equipment. According to the analysis, it is supposed that ZnO-C_3N monolayer is qualified to be used in maintaining insulation strength and ensuring the safe operation of power system.

Keywords: C_3N monolayer, Metal oxide modification, Density functional theory, SF_6 decomposed species

Introduction

With the rapid development of nanotechnology, the application of sensors based on novel nanomaterials is increasing in recent years. By virtue of its quick response, low consumption, low cost, and high sensitivity, nano-sensor has been exclusively studied in the field of medical, military, gas detection and environment monitoring [1–4]. Resistance-type sensor, as one of the most commonly used sensors, is favoured by scholars because of its simple structure and working mechanism. In the early stage, the graphene is an attractive material in gas detection for its excellent performance on physical and chemical, such as large specific surface area, high carrier mobility, and favourable heat conductivity [5–8]. However, the graphene is limited in the application of gas recognition due to its zero bandgap characteristic [9, 10], underperforming in identifying common gases like CO, CO_2, CH_4, N_2, NO_2, NH_3, H_2, and H_2O [11]. Afterwards, with the joint effort of scholars, numerous novel nanomaterials with the same properties to graphene but free from zero bandgap have sprung up in the field of gas sensing, including but not limited to transition metal dichalcogenides (TMDs) [12–14], metal carbides and nitrides [15], layered group III-VI semiconductors [16, 17], and group III-V nitrides [18–20].

Among the new emerged graphene-like materials, C_3N is synthesized by the direct pyrolysis of hexaaminobenzene trihydrochloride single crystals or the polymerization of 2, 3-diaminophenazine [21, 22], which has attracted considerable attention as a gas adsorbent [23–25]. The C_3N is intrinsically an indirect semiconductor with the bandgap of 0.39 eV that can be tuned by fabrication of quantum dots with different diameters [22]. In micro appearance, C_3N can be regarded as a 2 × 2 graphene supercell substituted by two nitrogen atoms, possessing a planar

* Correspondence: xiaoxing.zhang@outlook.com
[1]School of Electrical Engineering and Automation, Wuhan University, Wuhan 430072, China
[2]Hubei Key Laboratory for High-efficiency Utilization of Solar Energy and Operation Control of Energy Storage System, Hubei University of Technology, Wuhan 430068, China
Full list of author information is available at the end of the article

honeycomb lattice with six carbon atoms and two nitrogen atoms. As a result of the added N atoms, the intrinsic C_3N shows stronger chemical activity and higher carrier mobility but keeps similar structural stability compared to graphene, making the C_3N monolayer a competitive candidate for gas detection [26]. In terms of the adsorption ability, researchers have proved that the intrinsic C_3N has excellent selectivity and sensitivity [27] in detecting NO_2 and SO_2, while for other gases, there is no obvious adsorption effect. Nevertheless, research makes clear that the surface reactivity of C_3N could be largely promoted by the modification of impurity particles. For instance, Pashangpour and Peyghan [28] carried out a comparative experiment on CO adsorption ability of intrinsic and doped C_3N nanosheet; their results illustrate that Al dopant can bring about much stronger binding interaction than the pristine C_3N. Later, Zargham Bagheri [29] theoretically studied Si-doped C_3N for adsorption of acetone, and it is found by replacing a C atom with a Si atom, adsorption energy can increase from − 9.7 to − 67.4 kcal/mol, and the sensitivity increases as more C atoms are substituted.

Metal oxide is a commonly used alternative in surface-modification to enhance the chemical reactivity for gas interactions. As one of the metal oxide semiconductors, ZnO has a bandgap of about 3.37 eV with exciting binding energy of about 60 meV, chemical stability, excellent photocatalytic properties, and high activity to some specified gases [30]. According to Ref [31], ZnO can grow in 0-dimensional (0D), 1-dimensional (1D), and 2-dimensional (2D) nanostructure morphologies, with examples of each class including nanoclusters, nanowires/nanotubes, and nanosheets/nanoribbons, respectively. Given the characteristic of easily controlled size and morphology [32, 33], ZnO nanoparticle is a promising material in working as a dopant to improve the sensing performance of nano-surfaces [34–36]. Recently, a few scholars have proposed theoretical studies on improving surface activity of nanomaterials by using single-molecule metal oxide dopant. E. Mohammadi-Manesh et al. [37] investigated the adsorption ability of Cu- and CuO-decorated graphene upon H_2S theoretically and found the conductivity of the modified graphene changed significantly compared to that of intrinsic graphene after the adsorption of H_2S. Asadi and Vaezzadeh [38] designed a B- and CuO-decorated graphene sheet for detecting H_2S and CO based on density functional theory (DFT). The simulation in these works was carried out by DFT and its computational codes extend the atomic or molecular structure periodically based on the defined supercell and then calculate the physical properties of the entire system. Based on this method, the adsorption of an atom or molecule on the substrate as a sensor is used to study nanostructures. The foregoing reports stimulate us to perform related and further research on this topic about single metal oxide molecule doping; herein, we doped C_3N with ZnO molecule instead of ZnO nanoparticle as a simplification to explore the effect of ZnO on gas sensing.

SF_6 is a widely used medium in gas insulated switchgear (GIS) with prominent insulating and arc-extinguishing properties [39]. The inevitable accident inner defects, such as partial discharge (PD) in GIS, will decompose SF_6 to some low-fluoride sulphides such as SF_4, SF_3, and SF_2 [40]. These by-products would further react with the trace moisture and oxygen, generating some stable chemicals such as H_2S, SO_2, SOF_2, and SO_2F_2 [41]. The insulating reliability of these by-products is much lower than SF_6 and their existence will accelerate PD evolution if left alone. Therefore, so as to guarantee the safe operation of GIS, it is essential to detect or sweep away these gases. In this paper, we chose ZnO as a dopant and built the model of ZnO-modified C_3N (ZnO-C_3N) monolayer to study its adsorption performance upon typical SF_6 decomposed species (H_2S, SO_2, SOF_2, and SO_2F_2) theoretically. By analysing the structural changes, electron transfer behaviour, band structure, and density of state (DOS), the impact of ZnO dopant on interaction between the C_3N surface and gas molecules were comprehensively studied. The purpose of our work is to give detailed adsorption and sensing mechanism of ZnO-C_3N monolayer for potential application to detect or scavenge the impurity gases in the SF_6 insulation devices.

Computational Details

All of the calculations based on DFT were carried out in $Dmol^3$ package [42]. For the sake of better describing the non-uniform electron density of realistic system, we employed the generalized gradient approximation (GGA [43]) within the Perdew-Burke-Ernzerhof (PBE) function and the dispersion correction of TS to deal with the electron exchange-correlation terms [44, 45]. The DFT semi-core pseudopots (DSSP) was induced for core treatment and double numeric basis with polarization (DNP) was chosen as the atomic orbital basis set [46]. Monkhorst-Pack *k*-points of 6 × 6 × 1 meshes were defined in both geometric optimization and electronic structure calculations [47]. The energy convergence tolerance, maximum force, and maximum displacement in geometric optimization were respectively set as 1.0×10^{-5} Ha, 0.002 Ha/Å, and 0.005 Å [48]. Besides, the monolayer and its neighbouring image were separated by a vacuum spacing of 15 Å to avoid the interaction between them.

As illustrated in Fig. 1, the 2 × 2 × 1 supercell of C_3N monolayer and the gas molecules were established and optimized prior to the doping and adsorption process. The C-N bond (1.422 Å) in the optimized monolayer is slightly longer than C-C bond (1.418 Å) as a consequence

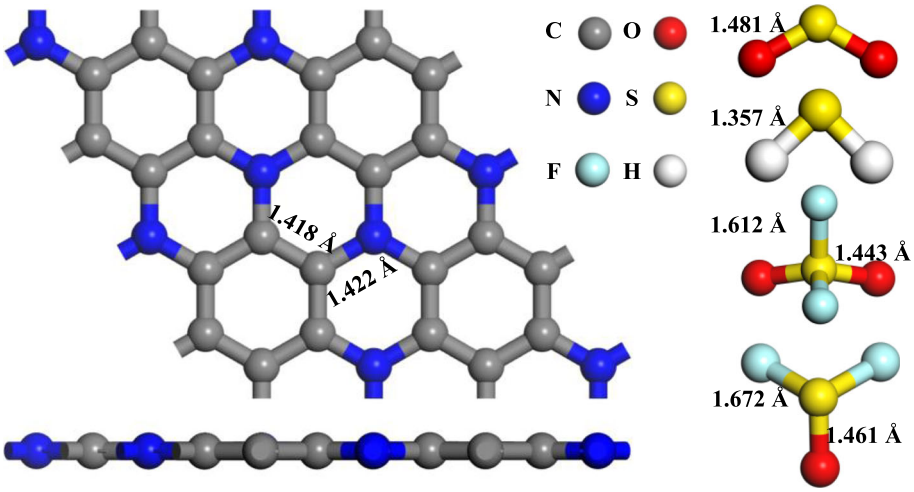

Fig. 1 Optimized structure of C_3N monolayer, H_2S, SO_2, SOF_2, and SO_2F_2

of the larger radius of N atom in comparison with C atom. The lattice constant obtained in this work is 4.92 Å, similar to the reported results in Ref. [25, 49]. We calculated the charge transfer between the molecule and monolayer by Hirshfeld analysis and defined Q_T to represent the charge change in the gas molecule. A positive Q_T indicates the electron-releasing behaviour of the gas molecule. Oppositely, it suggests the electron receiving behaviour of the gas molecule.

Results and Discussion

Analysis of ZnO-Modified C_3N Monolayer

After geometric optimization, the ZnO was placed on the surface of C_3N monolayer in different orientations and position to explore the most reasonable configuration of ZnO-C_3N. According to Fig. 2a, ZnO particle is approaching C_3N monolayer through the vertical (O_1, O_2) and parallel (O_3) orientations to the plane at the position of the centre of the hexagonal structure (P_{H1}, P_{H2}), the middle point of the C-C and C-N bonds (P_{B1}, P_{B2}), and right above the C atom (P_C) and N atom. We defined formation energy (E_{form}) to assess the stability of ZnO-C_3N monolayer, calculated as follows:

$$E_{\text{form}} = E_{\text{ZnO-C}_3\text{N}} - E_{\text{ZnO}} - E_{\text{C}_3\text{N}} \quad (1)$$

where E_{ZnO} and E_{C_3N} are the energy of ZnO molecule and C_3N monolayer before doping, and E_{ZnO-C_3N} is the energy of ZnO-C_3N structure. When the close-range "bonding" between atoms occurs in the extended atomic structure, the total energy is reduced and resulting in a negative E_{form} [50]; the structure with the largest E_{form} is selected for adsorption and further analysis.

All the configurations of ZnO-C_3N monolayer are displayed in Figure S1, S2, S3. These results demonstrate that most of the structures with large E_{form} are in O_2 orientation and the ZnO particle prefers to approach the C_3N surface by O-oriented position and trapped by a C atom. Furthermore, each modification process in this study is spontaneous since the E_{form} is negative and the maximum E_{form} is obtained by placing the ZnO particle at S_C in O_2 orientation. As can be seen in Fig. 2b, the diatomic molecule is attached to C_3N with a tilt of 40°. The Zn-O bond is elongated from 1.733 Å to 2.182 Å and the C-O bond is measured as 1.338 Å. Under the effect of ZnO, the surface of C_3N is no longer flat but a certain degree of distortion occurs, and meanwhile the C atom nearest to O atom is pulled out of the surface. For further discussion of the electronic behaviour of ZnO-C_3N monolayer, the deformation charge density (DCD) and density of state (DOS) are depicted in Fig. 3. In Fig. 3a, the red region corresponds to an increase in charge density and the decrease is represented in blue. When ZnO molecule is adsorbed, it extracts 0.255 e from the C_3N monolayer and a distinct red area can be recognized around the O atom. While the Zn atom is surrounded by a blue area, signifying the difference in electronegativity between O atom and Zn atom. Moreover, the significant raise of charge density between O atom and C atom suggest the formation of C-O bond which can also be supported by the intense hybridization between the states of O 2p orbital and that of C 2p orbital, as shown in Fig. 3c. From the DOS curve in Fig. 3b, it is obvious that the introduction of ZnO leads to an increase in the systemic DOS and the appearance of several novel peaks. It can be identified that the new emerged small peaks are contributed by the O atom at about − 2.5 eV and the biggest one

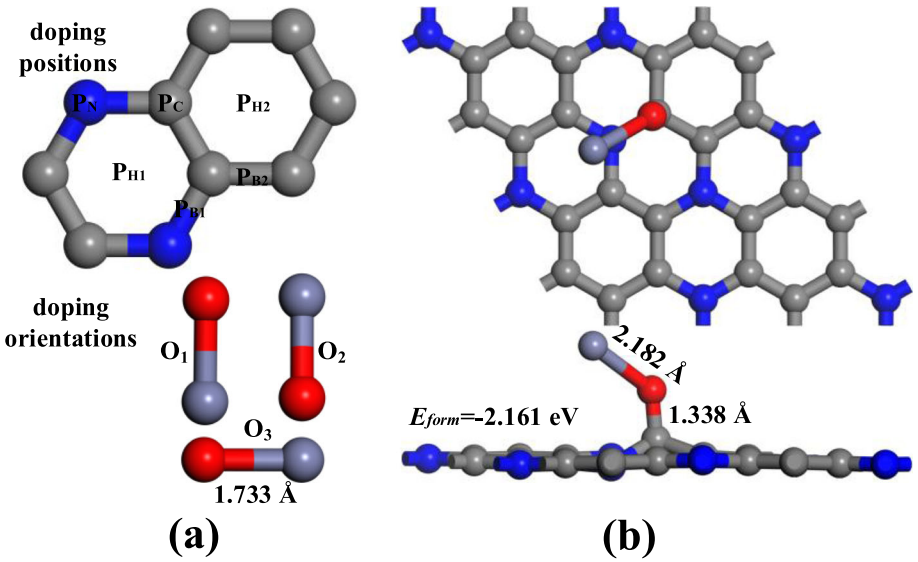

Fig. 2 **a** The approaching positions and orientations of ZnO molecule. **b** The most stable configuration of ZnO-C_3N

located at − 5.6 eV apparently resulted from the Zn 3d orbital. The changes in DOS and the hybridization between orbitals confirmed the fact that the ZnO particle have firmly adsorbed on the surface of C_3N and exerted great impact on the electronic structure of the whole system.

Adsorption Behaviour of ZnO-C_3N Monolayer

To fully compare the possible adsorption parameters and select the most desirable configuration for analysis, we put each gas molecule above the surface of ZnO-C_3N monolayer in various orientations. For example, for triatomic molecules, namely H_2S and SO_2, we made the plane

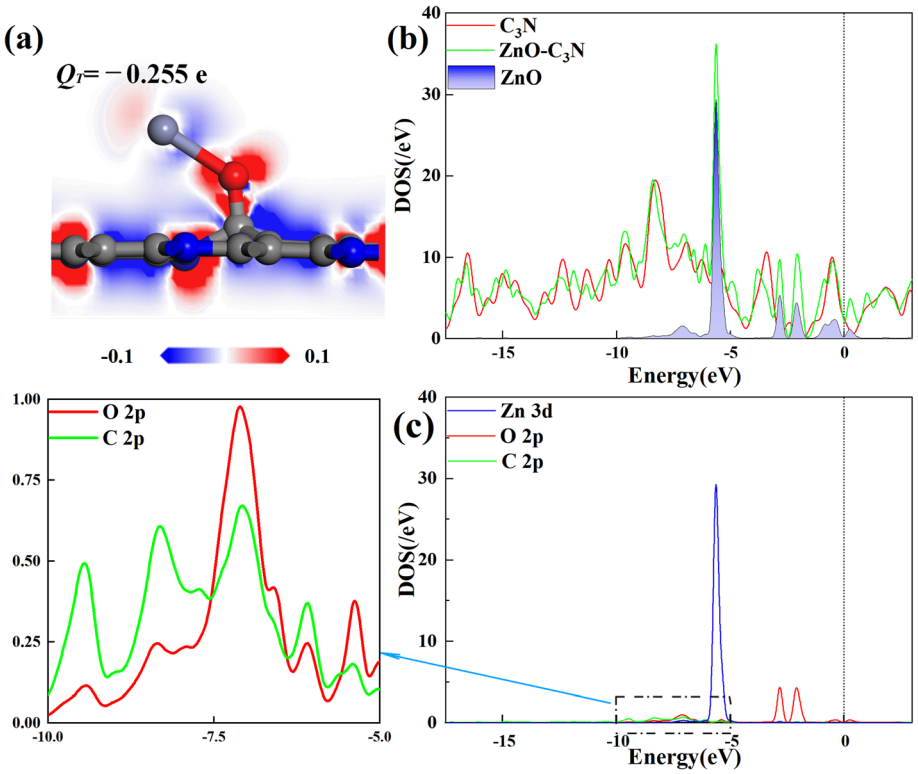

Fig. 3 **a** DCD and **b**, **c** DOS and PDOS of ZnO-C_3N monolayer

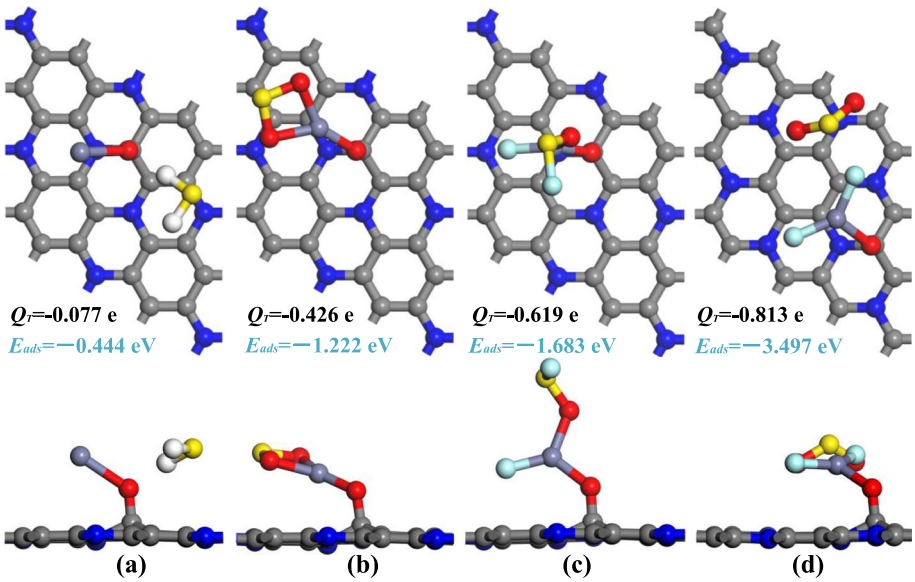

Fig. 4 The adsorption configuration of **a** H_2S system, **b** SO_2 system, **c** SOF_2 system, and **d** SO_2F_2 system

composed of the three atoms parallel or vertical to the surface with the S atom upward or downward. The adsorption energy (E_{ads}) is employed to describe the energy changes of different adsorption structures and calculated as

$$E_{\mathrm{ads}} = E_{\mathrm{ZnO\text{-}C_3N/gas}} - E_{\mathrm{ZnO\text{-}C_3N}} - E_{\mathrm{gas}} \quad (2)$$

where E_{gas} and $E_{\mathrm{ZnO-C_3N}}$ are the energy of the isolated gas molecule and the ZnO-C_3N monolayer before adsorption, $E_{\mathrm{ZnO-C_3N/gas}}$ represents the energy of the system with gas adsorbed. After the local minimum total energy of each situation was obtained, only the structure with the maximum E_{ads} was chosen for further discussion, as given in Fig. 4, and the electron density difference (EDD) is portrayed in Fig. 5 for better understanding of the charge transfer mechanism.

The H_2S adsorption system is given in Fig. 4a, wherein H_2S molecule is adsorbed in parallel position and the nearest atomic distance between H_2 molecule (H atom) and ZnO dopant (O atom) is measured as 2.042 Å. The H-S bond of the capture H atom is elongated to 1.374 Å

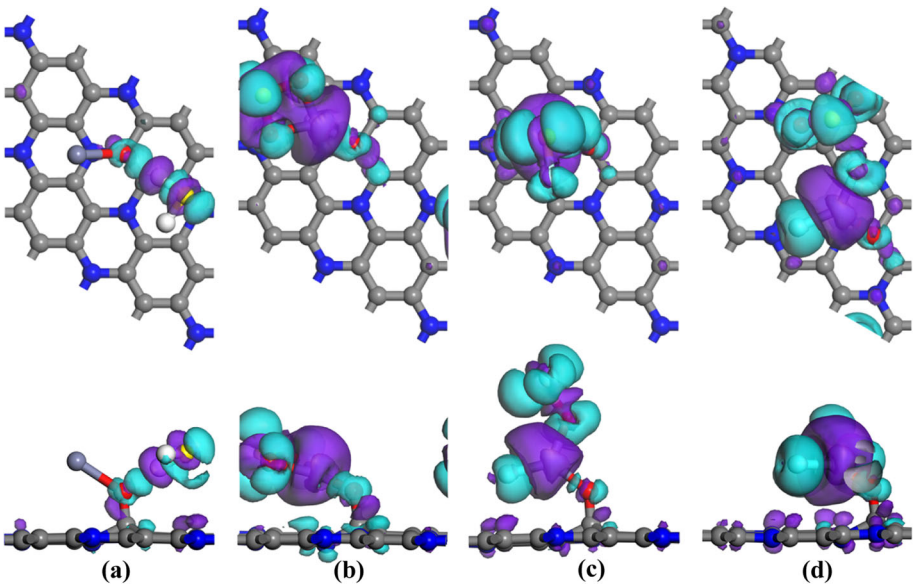

Fig. 5 The EDD of **a** H_2S system, **b** SO_2 system, **c** SOF_2 system, and **d** SO_2F_2 system

compared with the 1.357 Å in its isolated state, while the other H-S remains unchanged during the adsorption process. The slight deformation of the geometry configuration suggests the interaction between H_2S molecule and ZnO-C_3N monolayer is weak. Combined with the E_{ads} (– 0.444 eV) and Q_T (– 0.077 e), it is clear that H_2S molecule cannot stably adhere to ZnO-C_3N monolayer; we assume that ZnO-C_3N monolayer is unsuitable for detecting H_2S. For the SO_2 molecule shown in Fig. 4b, both O atoms are trapped by Zn atom with the distance of 2.020 and 2.031 Å, respectively. The ZnO particle bends closer to the surface and the angle formed by Zn-O-C is reduced from 129 to 118° due to the presence of SO_2. At the same time, from the Hirshfeld analysis, we find that the S atom acts as an electron donator with a loss of 0.164 e and its adsorption effect to O atoms is weakened, resulting in the extension of S-O bonds from 1.481 to 1.619 Å [51]. Inversely, the strengthened interatomic force, because of the electron increase (0.292 e) in the O atom of ZnO, has shortened the Zn-O bond from 2.182 to 1.869 Å. Apart from the geometric variations and electron transfer, the E_{ads} up to – 1.222 eV is another evidence of strong interaction during the adsorption process, indicating potential application of ZnO-C_3N monolayer in detecting SO_2. As for the SOF_2 and SO_2F_2 adsorption system given in Fig. 4c and d, it can be seen that the target molecules have undergone dramatic change in morphology. The F atom in SOF_2 gets rid of the constraint of S-F bond and adsorbed by Zn atom at a distance of 1.830 Å. An even more drastic change can be observed in SO_2F_2 where both of the S-F bonds broke and formed Zn-F bonds with the lengths of 1.802 and 1.883 Å. In addition to the formation of Zn-F bond, the remaining SOF group in SOF_2 system is also trapped by the Zn atom through Zn-O bond. But in the case of SO_2F_2 system, it is interesting to note that the SO_2 group generated by the decomposition of SO_2F_2 is not captured but keeps a distance from Zn atom, and with its S-O bonds calculated the same as isolated SO_2 in length. The pronounced deformation of gas molecules is associated with the large E_{ads} calculated as large as – 1.683 eV in SOF_2 system and – 3.497 eV in SO_2F_2 system. Based on this, the adsorption of SOF_2 and SO_2F_2 onto ZnO-C_3N can be determined as strong chemisorption accompanied by a large amount of charge transfer in this process, indicating the possible existence of significant electron orbital hybridization. With the large E_{ads} and Q_T, ZnO-C_3N monolayer can provide more stable adsorption to SO_2, SOF_2, and SO_2F_2 than other nanomaterials, as listed in Table 1, the adsorption configuration of ZnO-C_3N monolayer is larger than the listed nanomaterials by 0.358–3.281 eV and 0.038–0.811 e, ensuring the adsorption performance of this material when used in gas detection, whereas we speculate that it is hard for these gas molecules (SO_2, SOF_2 and SO_2F_2) to get rid of the strong interaction force as a consequence of the large E_{ads}. Hence, in order to prevent the performance degradation caused by sensor poisoning, measures such as high-temperature annealing or ultraviolet radiation should be taken to improve the desorption performance of the ZnO-C_3N monolayer. The specific desorption performance analysis will be provided in the "Gas sensing performance evaluation" section.

In terms of the EDD shown in Fig. 5, the blue part indicates the electron accumulation region and the other part in purple is the electron depletion region. For H_2S system, a small accumulation region can be found between H atom and O atom, while most of the accumulation and depletion regions are located around the H_2S molecule, suggesting the small charge transfer and the redistribution of molecular orbitals in H_2S molecule. In the SO_2 adsorption system, there are obvious depletion regions that surround the S atom and Zn atom, whereas the accumulation regions are mainly distributed around O atoms and above S atom. This phenomenon confirms the electron receiver role of SO_2 molecule, in accordance with the Q_T (– 0.426 e) obtained from Hirshfeld analysis. In SOF_2 and SO_2F_2 systems, judging from the large scale of accumulation and depletion regions, there are remarkable charge transfers and electron hybridization in

Table 1 The adsorption configuration comparison of ZnO-C_3N monolayer and other nanomaterials

Substrate	Gas	E_{ads}/eV	Q_T/e	Substrate	Gas	E_{ads}/eV	Q_T/e
ZnO-C_3N	SO_2	**– 1.222**	**– 0.426**	Ni-BNNT [52]	SO_2	– 0.864	0.105
	SOF_2	**– 1.683**	**– 0.619**		SOF_2	– 0.522	0.078
	SO_2F_2	**– 3.497**	**– 0.813**		SO_2F_2	– 0.223	– 0.035
C_3N [27]	H_2S	– 0.230	– 0.004	Ni-ZnO [53]	SO_2	– 0.245	– 0.086
	SO_2	– 0.620	– 0.23		SOF_2	– 0.207	0.016
	NO_2	– 0.790	– 0.388		SO_2F_2	– 0.219	0.003
Au-TiO_2 [54]	SO_2	– 0.657	– 0.156	Au-MoS_2 [55]	SO_2	– 0.946	– 0.222
	SOF_2	– 0.593	– 0.006		SOF_2	– 0.332	– 0.095
	SO_2F_2	– 0.200	0.039		SO_2F_2	– 0.175	0.002

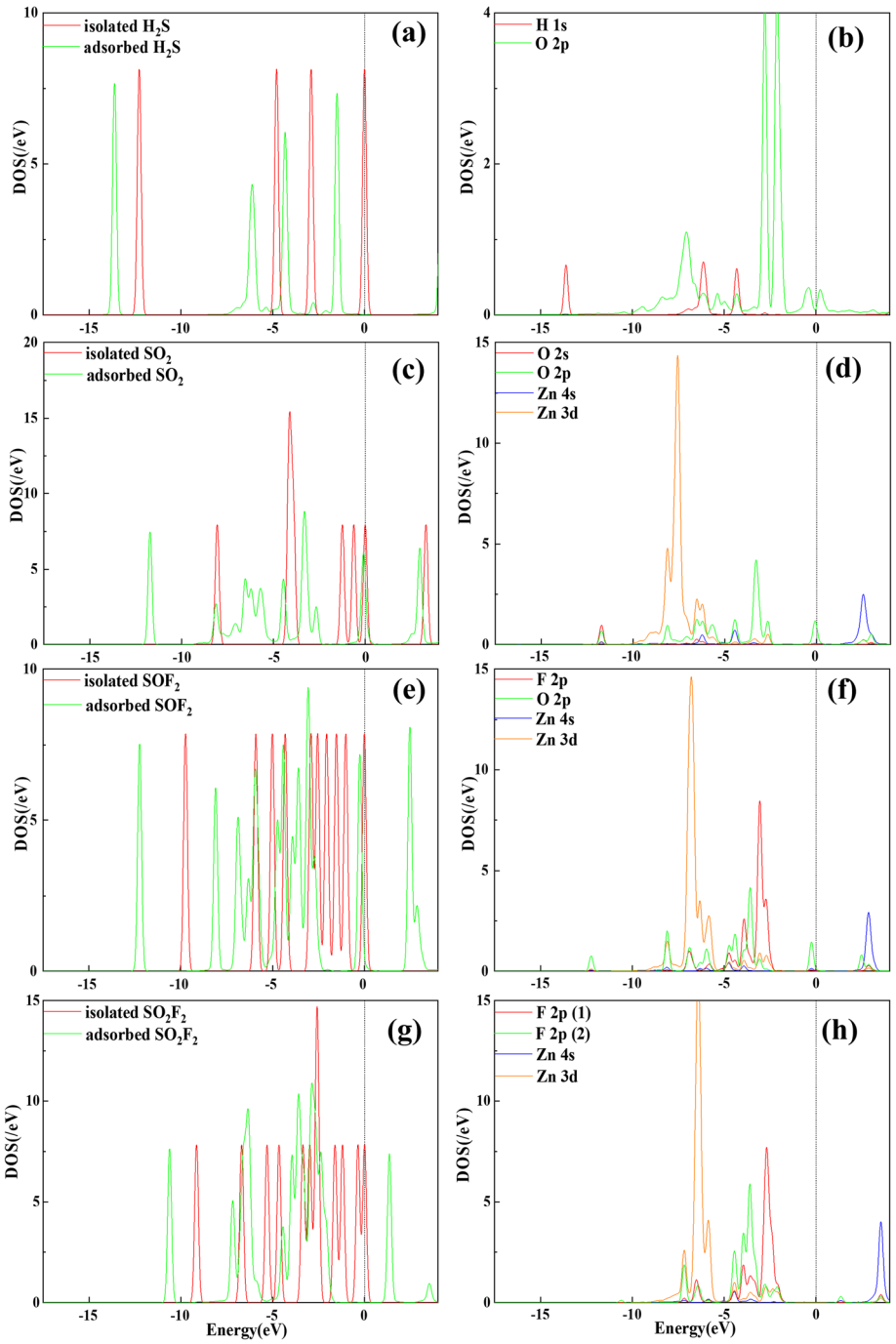

Fig. 6 DOS and PDOS of the gas molecule adsorbed on ZnO-C_3N monolayer. **a**, **b** H_2S system. **c**, **d** SO_2 system. **e**, **f** SOF_2 system. **g**, **h** SO_2F_2 system

both systems. The accumulation regions are distributed among the atoms of the target gas, while the depletion regions are mainly localized around Zn atom, reflecting the distinct electron-donating property of Zn atom. As a result, these electronic behaviours make the assumption that the ZnO-C_3N monolayer has strong adsorption to the gas molecules more persuasive.

Electronic Properties of ZnO-C_3N Monolayer on Gas Adsorption

As reported in graphene- [56], SWCNT- [57], and $MoSe_2$- [58] based gas sensing researches, DOS is another important parameter in investigating the electronic behaviour between gases and nanostructure. It can be seen in Fig. 6a that the redistribution of the molecular

orbitals in H_2S is in accord with the conclusion derived from the EDD in Fig. 5a. The hybridization between the H 1s and O 2p orbitals is available near − 4 and − 6 eV but of a low degree, demonstrating the weak interaction and the tiny possibility in forming a new H-O bond. As to the SO_2 system in Fig. 6c, the antibonding orbital slightly moves near the Fermi level and part of the orbitals transforms from separation to connection, manifesting the apparent redistribution of the electronic structure in SO_2 molecule. For the interaction between the atoms in Fig. 6d, the O 2p, Zn 4s, and Zn 3d orbitals are found hybridized at multiple energy levels, such as − 6, − 4, and − 2 eV. The hybridization signifies the strong chemical interaction between O atom and Zn atom and effectively supports the formation of Zn-O bond as calculated in the optimized structure. In the SO_2F and SO_2F_2 system, due to the dramatic deformation in structure, the molecular orbitals are strongly activated and redistributed with many new formed orbitals. The F 2p and O 2p orbitals in SOF_2 are intensely hybridized with the Zn 4s and 3d orbitals at − 8, − 7, and + 3 eV. The hybridization between F atoms and Zn atoms can be identified near − 7, − 5, and + 3.5 eV. The apparent hybridization between Zn atom and the trapped F, O atoms is the evidence of the formation of stable chemical bonds, namely the Zn-F and Zn-O bonds, which can be an explanation for the strong adsorption effect between ZnO-C_3N monolayer and the two gases. Combined with the results obtained from four adsorption systems, except for H_2S molecule, the other three molecules (SO_2, SO_2F, and SO_2F_2) can be firmly adsorbed when exposed to the ZnO-C_3N monolayer. This conclusion proves that the substance has the potential gas removal application in the high-voltage equipment.

Gas Sensing Performance Evaluation

To achieve the gas detection, a moderate change in conductivity is necessary for post-adsorption resistive-type devices. The conductivity of a certain system is related to its bandgap according to the following equation [59]:

$$\sigma = A \times e^{-E_g/2k_BT} \tag{3}$$

where A is a certain constant, k_B is the Boltzmann constant (8.62×10^{-5} eV K^{-1}) and T is the temperature. An inversely proportional relationship can be recognized between conductivity and bandgap, the wider the bandgap, the more difficult it is for electron to cross the forbidden band. Figure 7a demonstrates that the bandgap in ZnO-C_3N monolayer is pretty small as 0.168 eV which is less than half of the bandgap in pristine C_3N (0.39 eV), while the properties of semiconductor and indirect bandgap remain the same that can be judged from the different location of the bottom of conduction band (M) and the top of valence band (Γ). With respect to the bandgap of adsorption systems, different variations can be found in Fig. 7b–d. In H_2S system, the bandgap decreases to 0.125 eV on account of the downward movement in the bottom of conduction band. In other systems, the novel impurity level that appears at the top of valence band meets with the Fermi level near the M point and results in the zero bandgap of these systems, which can be considered strong p-type doping for the ZnO-C_3N monolayer [43, 60]. Although the semiconducting nature of the adsorbed structures may be covered by their metallic-like property of zero bandgap [61], the zero bandgap could provide visible enhancement in conductivity. It is much significant to improve the response performance of the devices based on ZnO-C_3N monolayer. To amplify further analysis of the response (R) performance, herein, we calculate it based on the following equation [62]:

$$R = \frac{\left|\frac{1}{\sigma_{\text{gas}}} - \frac{1}{\sigma_{\text{gas}}}\right|}{\frac{1}{\sigma_{\text{pure}}}} = \left|\frac{\sigma_{\text{pure}} - \sigma_{\text{gas}}}{\sigma_{\text{gas}}}\right| \tag{4}$$

where σ_{pure} and σ_{gas} represent the conductivity of the ZnO-C_3N system before and after adsorption, respectively. According to the calculations, the R for the H_2S system and the rest three systems are 0.567 and 0.962,

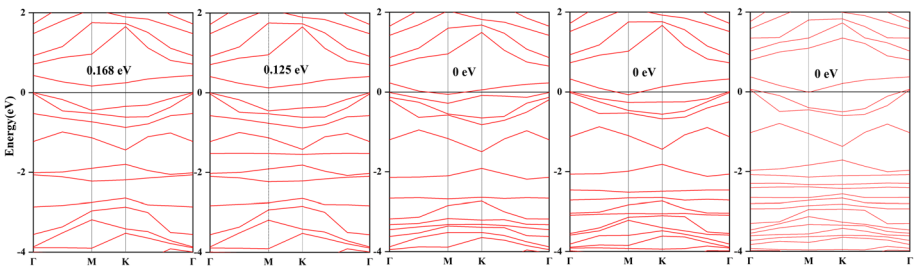

Fig. 7 Band structure of **a** ZnO-C_3N monolayer, **b** H_2S system, **c** SO_2 system, **d** SOF_2 system, and **e** SO_2F_2 system

Table 2 The recovery time of ZnO-C_3N towards H_2, CH_4, and C_2H_2 at different temperature

Temperature (K)	τ-H_2S (s)	τ-SO_2 (s)	τ-SOF_2 (s)	τ-SO_2F_2 (s)
298	3.15×10^{-5}	4.70×10^{8}	2.81×10^{16}	1.33×10^{47}
398	4.11×10^{-7}	3.01×10^{3}	2.00×10^{9}	1.85×10^{32}
498	3.07×10^{-8}	2.34	1.06×10^{5}	2.39×10^{23}
598	5.45×10^{-9}	0.02	150.29	2.90×10^{17}
698	1.59×10^{-9}	6.70×10^{-4}	1.40	1.74×10^{13}

namely the conductivity would increase by 56.7% and 96.2% when the adsorption occurs on the surface of ZnO-C_3N monolayer; in this case, it is possible to detect the existence of these gases.

The recovery time (τ) is another important parameter to estimate the property of sensors used in gas detection, which indicates the time spent in removing the adsorbed gas molecules. By reviewing the literature, τ could be calculated by the van't Hoff Arrhenius equation [63]:

$$\tau = F^{-1} e^{-E_a/k_B T} \quad (5)$$

where F is the attempt frequency and defined as $10^{12}\ s^{-1}$ in this study. E_a is the energy barrier for desorption which is assumed the same as the value of E_{ads} here, k_B and T are defined the same as in Eq. (3). From the Eq. (5), desorption for the adsorbed gases would be harder as the E_{ads} getting larger, but it can also be controlled by raising the working temperature.

Table 2 lists the recovery time required for the four gases to remove from the surface of ZnO-C_3N monolayer. For the H_2S molecule, the small E_{ads} undoubtedly reflects the low energy barrier for desorption, accordingly, causing the extra short recovery time in microseconds. At the meantime, for the systems with larger E_{ads}, it seems impossible to separate the gas molecule from the surface at the working temperature as the desorption will takes several days. When it reaches 498 K and 598 K which can rarely occur in the electrical equipment, the desorption process could be accelerated to the minutes scale for SO_2 and SOF_2, respectively. The extremely strong adsorption between the gas molecules (SO_2, SOF_2, and SO_2F_2) and the surface reveals the potential application of the ZnO-C_3N monolayer as a gas scavenger to remove the SF_6 decomposition species and maintain the good insulation state inside the power system. In addition, in the actual structure, given the high quantity of ZnO nanocrystals on C_3N, the effect is expected to be substantially enhanced. Besides, comparing to the original configuration, the activity of the gases releasing from the ZnO-C_3N monolayer is greatly impaired and can hardly exert impact on the system because of the severe deformation of the molecular structures (SOF_2 and SO_2F_2). In terms of the H_2S, it is supposed that the unstable interaction and extremely short recovery time of ZnO-C_3N monolayer towards H_2S are unable to provide an effective detection as the adsorption density is supposed to be small.

Conclusions

In this paper, a model of ZnO-modified C_3N is established and the optimal structure is investigated by placing the ZnO particle on the surface of C_3N in various orientations and position. Thus, the adsorption parameters of the ZnO-C_3N monolayer on four SF_6 decomposition species, namely H_2S, SO_2, SOF_2, and SO_2F_2, were obtained by analysing the E_{ads}, DOS, Q_T, and band structure before and after adsorption. It is found that the H_2S molecule can hardly adsorb stably on the nanostructure; at the same time, the other gases are strongly trapped in the ZnO particle. These results confirmed that the adsorption performance of ZnO-C_3N monolayer allows its potential application as gas scavenger to sweep SO_2, SOF_2, and SO_2F_2 from the high-voltage equipment, which keeps the insulation strength and the safe operation of power system. Plus, the frontier molecular orbital theory implies that ZnO-C_3N monolayer possesses the possibility to estimate the dielectric state of SF_6 insulation equipment as an indicator, given the obvious changes in conductivity caused by the adsorption of the abovementioned gases.

Supplementary information

Supplementary information accompanies this paper at https://doi.org/10.1186/s11671-020-03412-y.

Additional file 1: Figure S1. The initial positions and optimized structure of ZnO-C_3N with the symmetry axis of ZnO vertical to the plane (O_1). **Figure S2.** The initial positions and optimized structure of ZnO-C_3N with the symmetry axis of ZnO vertical to the plane (O_2). **Figure S3.** The initial positions and optimized structure of ZnO-C_3N with the symmetry axis of ZnO parallel to the plane (O_3).

Authors' Contributions

Writing—original draft preparation, P.W. Writing—review and editing, X.Z. and D.C. Funding acquisition, J.T. The authors read and approved the final manuscript.

Funding

This research was funded by the National Natural Science Foundation of China under grant 51777144.

Availability of Data and Materials

All the data and material are provided in the manuscript and supplementary file.

Competing Interests

The authors declare no conflict of interest.

Author details

[1]School of Electrical Engineering and Automation, Wuhan University, Wuhan 430072, China. [2]Hubei Key Laboratory for High-efficiency Utilization of Solar Energy and Operation Control of Energy Storage System, Hubei University of Technology, Wuhan 430068, China. [3]State Key Laboratory of Power Transmission Equipment & System Security and New Technology, Chongqing University, Chongqing 400044, China.

Received: 11 June 2020 Accepted: 14 September 2020
Published online: 25 September 2020

References

1. Altmann J, Gubrud M (2004) Anticipating military nanotechnology. IEEE Technol Soc Mag 23:33–40
2. Cui H, Zhang X, Zhang J, Zhang Y (2019) Nanomaterials-based gas sensors of SF6 decomposed species for evaluating the operation status of high-voltage insulation devices. High Volt 4:242–258
3. Nair LV, Philips DS, Jayasree RS, Ajayaghosh A (2013) A near-infrared fluorescent nanosensor (AuC@Urease) for the selective detection of blood urea. Small 9:2673–2677
4. Xu S, Hansen BJ, Wang ZL (2010) Piezoelectric-nanowire-enabled power source for driving wireless microelectronics. Nat Commun 1:93
5. Berger C, Song Z, Li T, Li X, Ogbazghi A, Feng R, Dai Z, Marchenkov A, Conrad E, First P, de Heer W (2004) Ultrathin epitaxial graphite: 2D electron gas properties and a route toward graphene-based nanoelectronics. J Phys Chem B 108:19912–19916
6. Stankovich S, Dikin DA, Dommett GHB, Kohlhaas KM, Zimney EJ, Stach EA, Piner RD, Nguyen ST, Ruoff RS (2006) Graphenebased composite materials. nature 442:282-286.
7. Stankovich S, Dikin DA, Dommett GHB, Kohlhaas KM, Zimney EJ, Stach EA, Piner RD, Nguyen ST, Ruoff RS (2006) Graphene-based composite materials. Nature 442:282–286
8. Yang S, Jiang C, Wei Sh (2017) Gas sensing in 2D materials. Applied Physics Reviews 4:021304
9. Robinson JT, Perkins FK, Snow ES, Wei Z, Sheehan PE (2008) Reduced graphene oxide molecular sensors. Nano Lett 8:3137–3140
10. Lu G, Ocola LE, Chen J (2009) Reduced graphene oxide for room-temperature gas sensors. Nanotechnology 20:445502
11. Cui H, Yan C, Jia P, Cao W (2020) Adsorption and sensing behaviors of SF6 decomposed species on Ni-doped C3N monolayer: a first-principles study. Appl Surf Sci 512:145759–145765
12. Hien ND, Cuong NQ, Bui LM, Dinh PC, Nguyen CV, Phuc HV, Hieu NV, Jappor HR, Phuong LTT, Hoi BD, Nhan LC, Hieu NN (2019) First principles study of single-layer SnSe2 under biaxial strain and electric field: modulation of electronic properties. Physica E Low Dimens Syst Nanostruct 111:201–205
13. Chen D, Zhang X, Xiong H, Li Y, Tang J, Xiao S, Zhang D (2019) A first-principles study of the SF6 decomposed products adsorbed over defective WS2 monolayer as promising gas sensing device. IEEE Trans Device Mater Reliab 19:473–483
14. Cui H, Jia P, Peng X (2020) Adsorption of SO2 and NO2 molecule on intrinsic and Pd-doped HfSe2 monolayer: a first-principles study. Appl Surf Sci 513:145863
15. Naguib M, Mochalin VN, Barsoum MW, Gogotsi Y (2014) 25th anniversary article: MXenes: a new family of two-dimensional materials. Adv Mater 26: 992–1005
16. Abed Al-Abbas SS, Muhsin MK, Jappor HR (2018) Tunable optical and electronic properties of gallium telluride monolayer for photovoltaic absorbers and ultraviolet detectors. Chem Phys Lett 713:46–51
17. Jappor HR (2017) Electronic structure of novel GaS/GaSe heterostructures based on GaS and GaSe monolayers. Physica B Condens Matter 524:109–117
18. Cui H, Zhang X, Li Y, Chen D, Zhang Y (2019) First-principles insight into Ni-doped InN monolayer as a noxious gases scavenger. Appl Surf Sci 494:859–866
19. Cui H, Liu T, Zhang Y, Zhang X (2019) Ru-InN monolayer as a gas scavenger to guard the operation status of SF6 insulation devices: a first-principles theory. IEEE Sensors J 19:5249–5255
20. Sajjad M, Feng P (2014) Study the gas sensing properties of boron nitride nanosheets. Mater Res Bull 49:35–38
21. Mahmood J, Lee EK, Jung M, Shin D, Choi HJ, Seo JM, Jung SM, Kim D, Li F, Lah MS, Park N, Shin HJ, Oh JH, Baek JB (2016) Two-dimensional polyaniline (C3N) from carbonized organic single crystals in solid state. Proc Natl Acad Sci U S A 113:7414–7419
22. Yang S, Li W, Ye C, Wang G, Tian H, Zhu C, He P, Ding G, Xie X, Liu Y, Lifshitz Y, Lee ST, Kang Z, Jiang M (2017) C3N-A 2D crystalline, hole-free, tunable-narrow-bandgap semiconductor with ferromagnetic properties. Adv Mater 29:1605625
23. Babar V, Sharma S, Schwingenschlögl U (2018) Highly Sensitive Sensing of NO and NO2 Gases by Monolayer C3N. Adv. Theory Simul 1:1700008
24. Eslami M, Moradi M, Moradi R (2016) DFT investigation of hydrogen adsorption on the C3N nanotube. Vacuum 133:7–12
25. Ma D, Zhang J, Li X, He C, Lu Z, Lu Z, Yang Z, Wang Y (2018) C3N monolayers as promising candidates for NO2 sensors. Sens Actuators B Chem 266:664–673
26. Zhou X, Feng W, Guan S, Fu B, Su W, Yao Y (2017) Computational characterization of monolayer C3N: a two-dimensional nitrogengraphene crystal. J Mater Res 32:2993–3001
27. Cui H, Zheng K, Zhang Y, Ye H, Chen X (2018) Superior selectivity and sensitivity of C3N sensor in probing toxic gases NO2 and SO2. IEEE Electron Device Lett 39:284–287
28. Pashangpour M, Peyghan AA (2015) Adsorption of carbon monoxide on the pristine, B- and Al-doped C3N nanosheets. J Mol Model 21:116
29. Bagheri Z (2016) DFT study on the chemical sensitivity of C3N nanotubes toward acetone. Physica E Low Dimens Syst Nanostruct 76:151–157
30. Chen D, Zhang X, Tang J, Cui H, Pi S, Cui Z (2018) Adsorption of SF6 decomposed products over ZnO(1010): effects of O and Zn vacancies. ACS Omega 3:18739–18752
31. Spencer MJS (2012) Gas sensing applications of 1D-nanostructured zinc oxide: insights from density functional theory calculations. Prog Mater Sci 57:437–486
32. Xu J, Pan Q, Shun YA, Tian Z (2000) Grain size control and gas sensing properties of ZnO gas sensor. Sens Actuators B Chem 66:277–279
33. Yang Y, Chen H, Zhao B, Bao X (2004) Size control of ZnO nanoparticles via thermal decomposition of zinc acetate coated on organic additives. J Cryst Growth 263:447–453
34. Hu Y, Zhou X, Han Q, Cao Q, Huang Y (2003) Sensing properties of CuO–ZnO heterojunction gas sensors. Mater Sci Eng B 99:41–43
35. Liu Y, Yu J, Lai PT (2014) Investigation of WO3/ZnO thin-film heterojunction-based Schottky diodes for H2 gas sensing. Int J Hydrogen Energy 39:10313–10319
36. Mohammadi-Manesh E, Rahmani S (2017) A theoretical study of ZnO-GS nanosensor to detect H 2 S at room temperature. Mater Chem Phys 192: 299–303
37. Mohammadi-Manesh E, Vaezzadeh M, Saeidi M (2015) Cu- and CuO-decorated graphene as a nanosensor for H2S detection at room temperature. Surf Sci 636:36-41
38. Asadi H, Vaezzadeh M (2017) Computational designing ultra-sensitive nano-composite based on boron doped and CuO decorated graphene to adsorb H2S and CO gaseous molecules. Mater Res Expr 4:075039
39. Beyer C, Jenett H, Klockow D (2000) Influence of reactive SFx gases on electrode surfaces after electrical discharges under SF6 atmosphere. IEEE Trans Dielect Electr Insul 7:234–240
40. Braun JM, Chu FY, Seethapathy R (1987) Characterization of GIS spacers exposed to SF6 decomposition products. IEEE Trans Elect Insul 22:187–193
41. Cui H, Zhang X, Zhang J, Tang J (2018) Adsorption behaviour of SF6 decomposed species onto Pd4-decorated single-walled CNT: a DFT study. Mol Phys 116:1749–1755
42. Delley B (2000) From molecules to solids with the DMol3 approach. J Chem Phys 113:7756–7764
43. Ma D, Wang Q, Li T, He C, Ma B, Tang Y, Lu Z, Yang Z (2016) Repairing sulfur vacancies in the MoS2 monolayer by using CO, NO and NO2 molecules. J Mater Chem C 4:7093–7101
44. Tkatchenko A, DiStasio RA Jr, Head-Gordon M, Scheffler M (2009) Dispersion-corrected Moller-Plesset second-order perturbation theory. J Chem Phys 131:094106
45. Perdew JP, Burke K, Ernzerhof M (1996) Generalized gradient approximation made simple. Phys Rev Lett 77:3865–3868
46. Delley B (2002) Hardness conserving semilocal pseudopotentials. Phys Rev B 66;1-9
47. Li X, Guo T, Zhu L, Ling C, Xue Q, Xing W (2018) Charge-modulated CO2 capture of C3N nanosheet: Insights from DFT calculations. Chem Eng J 338: 92–98
48. Cui H, Zhang X, Zhang G, Tang J (2019) Pd-doped MoS2 monolayer: a promising candidate for DGA in transformer oil based on DFT method. Appl Surf Sci 470:1035–1042
49. Zhou X, Feng W, Guan S, Fu B, Su W, Yao Y (2017) Computational characterization of monolayer C3N: a two-dimensional nitrogen-graphene crystal. J Mater Res 32:2993–3001
50. Leung KC-F, Li X-B, Li X, Lee S-F, Yu JC, Mendes PM, Hermann KE, Van Hove MA (2019) Soft nanohand grabs a growing nanoparticle. Mater Chem Front 3:1555–1564
51. He X, Gui Y, Xie J, Liu X, Wang Q, Tang CA (2020) DFT study of dissolved gas (C2H2, H2, CH4) detection in oil on CuO-modified BNNT. Appl Surf Sci. 500:144030

52. Pi S, Zhang X, Chen D, Tang J (2019) Sensing properties of Ni-doped boron nitride nanotube to SF6 decomposed components: A DFT study. AIP Advances 9:095101
53. Wang J, Zhou Q, Zeng W (2019) Competitive adsorption of SF6 decompositions on Ni-doped ZnO (100) surface: computational and experimental study. Appl Surf Sci 479:185–197
54. Zhang X, Dong X, Gui Y (2016) Theoretical and experimental study on competitive adsorption of SF6 decomposed components on Au-modified anatase (101) surface. Appl Surf Sci 387:437–445
55. Chen D, Zhang X, Tang J, Cui H. Li Y (2018) Noble metal (Pt or Au)-doped monolayer MoS2 as a promising adsorbent and gas-sensing material to SO2, SOF2 and SO2F2: a DFT study. Applied Physics A 124:194.
56. Zhang X, Yu L, Wu X, Hu W (2015) Experimental sensing and density functional theory study of H2S and SOF2 adsorption on Au-modified graphene. Adv Sci (Weinh) 2:1500101
57. Zhang X, Gui Y, Xiao H, Zhang Y (2016) Analysis of adsorption properties of typical partial discharge gases on Ni-SWCNTs using density functional theory. Appl Surf Sci 379:47–54
58. Cui H, Chen D, Zhang Y, Zhang X (2019) Dissolved gas analysis in transformer oil using Pd catalyst decorated MoSe2 monolayer: A first-principles theory. Sustainable Mater Technol 20:1-8
59. Li SS (2008) "Semiconductor physical electronics," Ed., Beijing: Science Press, Beijing
60. Li X, Li Y, Zhang X, Long M, Zhou G (2019) Spin-resolved electronic and transport properties of graphyne-based nanojunctions with different N-substituting positions. Nanoscale Res Lett 14:299
61. Sidike A, Guo G, Li X, Li D, Nie Y, Cao B, Duan H, Long M (2020) Spin dependent electronic transport properties of zigzag black phosphorene nanojunctions induced by Li H, Co O asymmetric edge saturations. Phys Letters A 384:126123
62. Cui H, Jia P, Peng X, Li P (2020) Adsorption and sensing of CO and C2H2 by S-defected SnS2 monolayer for DGA in transformer oil: A DFT study. Mater Chem Phys 249:123006
63. Zhang Y-H, Chen Y-B, Zhou K-G, Liu C-H, Zeng J, Zhang H-L, Peng Y (2009) Improving gas sensing properties of graphene by introducing dopants and defects: a first-principles study. Nanotechnology 20:185504

Publisher's Note